Determining dynamic content of turbulent reacting flow LES using the Lyapunov exponent

By J. W. Labahn, G. Nastac, L. Magri† AND M. Ihme

1. Motivation and objectives

Direct Numerical Simulation (DNS) and Large-Eddy Simulation (LES) have been employed for computing turbulent flows . While DNS resolves all turbulent scales involved in the dynamics with no physical modeling, LES represents the energy contained in the large scales, and effects of the smaller scales are taken into account either explicitly through a subgrid scale model or implicitly through the numerical dissipation of the numerical method. Besides numerical algorithms, two factors determine the quality of LES: the physical model or dissipation of the subgrid scales (SGS), which are filtered out in the governing equations, and the filter width, which describes the numerical resolution of the resolved scales.

Assessing the quality of LES has been the subject of numerous studies (Pope 2004; Celik *et al.* 2005; Vervisch *et al.* 2010). One commonly used statistical metric is Pope's criterion (Pope 2004),

$$M = \frac{k_{sgs}}{k_{res} + k_{sgs}} \,, \tag{1.1}$$

which is the ratio of subgrid turbulent kinetic energy, k_{sgs}, over the total turbulent kinetic energy, being the sum of the subgrid turbulent kinetic energy and the resolved turbulent kinetic energy, k_{res}. As a recommendation, Pope (2004) suggests that when $M \lesssim 0.2$, a simulation is sufficiently well-resolved. Although these types of statistical metrics are practical, LES is inherently unsteady and a dynamic measure is desirable to further characterize LES quality in representing the dynamic content of a simulation. The key observation is that turbulence is a deterministic chaotic phenomenon which is characterized by an aperiodic long-term behavior, exhibiting high sensitivity to the initial conditions. If a system is chaotic, given an infinitesimal initial perturbation to the solution, two trajectories of the system separate in time exponentially until nonlinear saturation. The average exponential separation is the Lyapunov exponent. A solution is typically regarded as chaotic if there exists at least one positive Lyapunov exponent. The Lyapunov exponent is (i) a robust indicator of chaos, (ii) a global quantity describing the strange attractors, since it does not depend on initial conditions for ergodic processes (Goldhirsch *et al.* 1987), and (iii) relatively simple to calculate (Boffetta *et al.* 2002). For these reasons, the first objective of this paper is to propose the Lyapunov exponent as a metric to evaluate the quality of LES in describing the chaotic dynamics of turbulent reacting flows. The second objective of this paper is to evaluate the effect that combustion has on the predictability of turbulent jets. The Lyapunov exponent as a dynamic quality index for LES is examined by considering a turbulent jet flame in which the turbulent combustion is represented using a manifold-based combustion model. Results from this simulation will be compared against a non-reacting jet-flow simulation

† University of Cambridge, UK

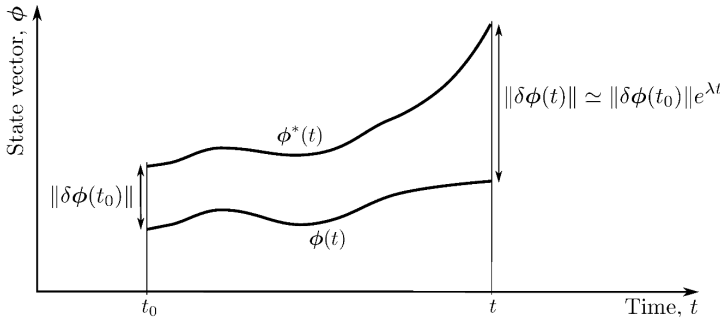

FIGURE 1. Solution separation of two slightly different solutions. The initial divergence is exponential and the growth rate is the Lyapunov exponent, λ.

that is performed at the same nozzle-exit conditions, thereby establishing a direct assessment of the combustion process on the turbulence dynamics through the Lyapunov metric (Nastac *et al.* 2017).

2. Lyapunov exponent

A turbulent flow can be represented as a dynamical system,

$$\dot{\boldsymbol{\phi}}(t) = \mathbf{F}[\boldsymbol{\phi}(t)], \tag{2.1}$$

with initial conditions $\boldsymbol{\phi}(t = t_0) = \boldsymbol{\phi}_0$; $\mathbf{F}$ is the set of bounded differentiable flow equations, $\dot{\boldsymbol{\phi}}$ denotes the temporal derivative of the state vector, which is denoted by $\boldsymbol{\phi}$. For a general chemically reacting flow, $\boldsymbol{\phi}$ contains the velocity vector, $(\boldsymbol{u})$, pressure, (p), density, (ρ), and vector of species mass fractions, $(\boldsymbol{Y})$: $\boldsymbol{\phi} = (\boldsymbol{u}, p, \rho, \boldsymbol{Y})^T$. The solution $\boldsymbol{\phi}(t)$ belongs to a vector space H, called the phase space. In the finite-dimensional case, $H \in \mathbb{R}^N$, where $N \in \mathbb{N}$. In the infinite-dimensional case H is a Hilbert space. The fluid dynamics problems studied are infinite-dimensional because they are governed by PDEs. However, they are characterized by the existence of a bounded set, called strange attractor, because they are dissipative systems. This means that the turbulent solution lies in a fractal set with finite dimension (Temam 1997). Moreover, after numerical discretization, the phase space necessarily becomes finite-dimensional. Hence, the fluid systems are considered finite-dimensional in this paper.

Consider two initial conditions, $\boldsymbol{\phi}_0$ and $\boldsymbol{\phi}_0^*$, which are infinitesimally distanced, $\boldsymbol{\phi}_0^* - \boldsymbol{\phi}_0 = \delta\boldsymbol{\phi}_0$ (see Figure 1 for a schematic illustration). The temporal evolution of the separation of the two trajectories, $\delta\boldsymbol{\phi}(t)$, in the tangent space, obeys the linearized dynamical equation

$$\delta\dot{\phi}_i(t) = \sum_{j=1}^{N_D} \frac{\partial F_i}{\partial \phi_j} \delta\phi_j(t_0), \tag{2.2}$$

where $i = 1, 2, \ldots, N_D$, with N_D being the number of degrees of freedom of the system, i.e., the dimension of the phase space. In the present study, $N_D \sim \mathcal{O}(10^7)$.

Under ergodicity, Oseledets (1968) proved that there exists an orthonormal basis $\{\mathbf{e}_j\}$ in the tangent space such that the solution can be expressed by a modal expansion,

$$\delta\boldsymbol{\phi}(t) = \sum_{j=1}^{N_D} \alpha_j \mathbf{e}_j e^{\lambda_j t}, \tag{2.3}$$

where the coefficients α_j depend on the initial condition $\delta\boldsymbol{\phi}(t_0)$. Mathematically, $\alpha_j = \langle \mathbf{e}_j, \delta\boldsymbol{\phi}(t_0)\rangle$, where the angular brackets denote an inner product. The exponents $\lambda_1 \geq \lambda_2 \geq ... \geq \lambda_{N_D}$ are the Lyapunov exponents. Customarily, the maximal Lyapunov exponent, λ_1, is referred to as the Lyapunov exponent and the subscript is omitted ($\lambda \equiv \lambda_1$). In the phase space, the modal expansion describes the deformation of an N_D-dimensional sphere of radius $\delta\boldsymbol{\phi}(t_0)$ centered at $\boldsymbol{\phi}(t_0)$ into an ellipsoid with semi-axes along the directions $\mathbf{e}_j$. Therefore, the Lyapunov exponents provide the stretching rates along these principal directions. Thus, given an infinitesimal initial perturbation to the solution, $\delta\boldsymbol{\phi}(t_0)$, the two trajectories of the system separate in time exponentially as (Boffetta *et al.* 2002)

$$\|\delta\boldsymbol{\phi}(t)\| \simeq \|\delta\boldsymbol{\phi}(t_0)\| e^{\lambda t}. \tag{2.4}$$

Figure 1 illustrates the significance of the Lyapunov exponent. The predictability time, t_p, of the system for infinitesimal perturbations is then defined as the inverse of the Lyapunov exponent

$$t_p = \ln\left(\frac{\|\delta\boldsymbol{\phi}(t)\|}{\|\delta\boldsymbol{\phi}(t_0)\|}\right)\frac{1}{\lambda} \sim \frac{1}{\lambda}. \tag{2.5}$$

2.1. *Calculation of the Lyapunov exponent as a separation growth rate*

The objective now is to utilize the Lyapunov exponent as an estimate for the rate of divergence of the Eulerian solution obtained by LES. From this information, a metric is proposed to measure how dynamically well-resolved the turbulent solution is. Using the Eulerian solution is a natural choice since most numerical simulations calculate Eulerian quantities. Growth rates of Eulerian fields have been used before in evaluating the error growth of weather models (Harlim *et al.* 2005) and finite perturbations of fully developed turbulence (Aurell *et al.* 1996). By observing that an Eulerian field can be regarded as a trajectory in an extended dynamical system (Aurell *et al.* 1996), a practical method for obtaining the Lyapunov exponent is to perturb the initial field $\boldsymbol{\phi}(t_0)$ as

$$\boldsymbol{\phi}_i^*(t_0) = \boldsymbol{\phi}_i(t_0) + \epsilon\,\|\boldsymbol{\phi}_i(t_0)\|\,, \tag{2.6}$$

where $\epsilon \ll 1$, $\|\cdot\| \equiv \left[(1/V)\int_V (\cdot)^p\, dV\right]^{1/p}$ is the L_p-norm, and V is the volume of the domain. The separation, also known as *error* (Harlim *et al.* 2005), is then measured by the L_p-norm of the subtracted Eulerian fields,

$$\|\delta\boldsymbol{\phi}\| = \|\boldsymbol{\phi}^*(t) - \boldsymbol{\phi}(t)\|\,. \tag{2.7}$$

The separation behaves in accordance to Eq. (2.4); thus, the Lyapunov exponent is computed as the linear slope of the natural logarithm of the separation versus time, $\lambda t = \ln\left(\|\delta\boldsymbol{\phi}(t)\|/\|\delta\boldsymbol{\phi}(t_0)\|\right)$. In the remainder of this work, the L_2-norm is chosen to measure the separation in Eq. (2.7).

If the process is ergodic, as assumed in this paper, the Lyapunov exponent is independent of the initial conditions as long as the nearly infinitesimal limit is satisfied (Oseledets 1968).

2.2. *Lyapunov metric for LES*

Compared to LES-quality metrics that rely on statistical information about turbulent kinetic energy or other flow-field quantities, the Lyapunov exponent intrinsically depends on the dynamic and chaotic nature of turbulence. While many turbulent flow systems of engineering interest are able to be time-averaged, some systems involve highly dynamic

flows that cannot be averaged. For example, rare events are particularly difficult to simulate and capture, such as preignition, extinction and cycle-to-cycle variations in internal combustion engines, using conventional turbulence modeling. As these rare events happen on a very small time scale, the simulations of these systems must be able to resolve the relevant dynamic. As shown subsequently, the Lyapunov exponent saturates when the dynamical scales of the problem saturate. Specifically, as the spatio-temporal resolution approaches the smallest physical scales, the magnitude of the Lyapunov exponent reaches a plateau. This, in turn, provides a robust evaluation of the resolution requirements in LES to capture the fundamental turbulent dynamics of rare deterministic events.

One caveat in using the Lyapunov exponent is that its asymptotic value is not known *a priori*; current results show that the value of the Lyapunov time scale correlates with the integral time scale. Iteration of resolution is likely required for more complex geometries and physics. The Lyapunov exponent is expected to be dependent on physical models and numerical discretization and can therefore be used as a sensitivity parameter and indicator to characterize their quality.

3. Turbulent jets

In this section, analysis of the Lyapunov exponent is applied to a turbulent jet flow. To gain fundamental understanding about the effect of combustion on the flow dynamics, studies on inert and reacting jets are performed.

3.1. *Model and computational setup*

LES of inert and reacting turbulent jets are performed. The operating conditions for the inert jet are chosen for comparison with experimental data (Mi *et al.* 2001). In this experiment, the jet is exiting from a pipe, and the length of the pipe is sufficiently long to ensure that the flow is fully developed when the fluid exits the nozzle. The jet-exit Reynolds number in this experiment is Re = 16,000, and the fluid exiting the nozzle is heated and behaves as a passive scalar.

A non-premixed jet flame configuration at similar operation conditions has been studied experimentally (Bergmann *et al.* 1998; Meier *et al.* 2000; Schneider *et al.* 2003). The burner configuration consists of a central fuel nozzle of diameter $D_{\mathrm{ref}} = 8$ mm, surrounded by a co-flow nozzle of square shape. The jet fluid consists of a mixture of 22.1 % CH_4, 33.2 % H_2, and 44.7 % N_2 by volume, with a stoichiometric mixture fraction of $Z_{\mathrm{st}} = 0.167$. The fuel bulk velocity is $U_{\mathrm{ref}} = 42.2$ m/s. Co-flowing air is supplied at an axial velocity of $7.11 \times 10^{-3} U_{\mathrm{ref}}$. The jet-exit Reynolds number is Re = 14,720. In the following, all quantities are non-dimensionalized appropriately, using U_{ref} and D_{ref}, and conditions of the jet flow.

The combustion is modeled by the flamelet/progress variable (FPV) approach (Pierce & Moin 2004). In this combustion model, all thermochemical quantities are parameterized by a three-dimensional reaction-diffusion transport manifold. For all reactive flow simulations, the reaction chemistry is described by the GRI 2.11 mechanism (Bowman *et al.* 1997), consisting of 279 reactions among 49 species. The governing equations are solved in a cylindrical coordinate system $\boldsymbol{x} = (x, r, \varphi)^T$. The computational domain is $120 D_{\mathrm{ref}} \times 45 D_{\mathrm{ref}} \times 2\pi$ in axial, radial, and azimuthal directions, respectively. A well-resolved LES pipe flow using the jet parameters is first simulated to obtain the inflow conditions for the flame. Convective outflow conditions are used at the outlet and no-slip boundary conditions are employed at the lateral boundaries. The domain is initialized

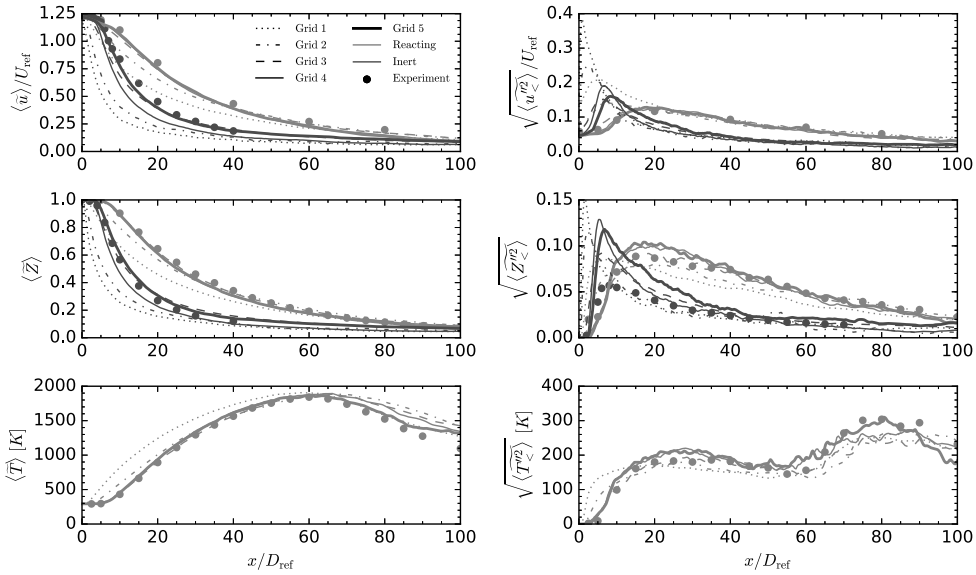

FIGURE 2. Resolved center-line statistics for the inert and reacting jets for axial velocity, mixture fraction, and temperature compared with experimental values (Mi *et al.* 2001; Bergmann *et al.* 1998; Meier *et al.* 2000; Schneider *et al.* 2003). Mean quantities on the left column; root-mean square quantities on the right column.

with the co-flow velocity and then advanced in time, using a CFL number of approximately 0.5. Once the inert jet reaches a statistically stationary state, the combustion model is turned on and the jet is advanced in time until it is statistically stationary. Large-eddy simulations of five grids, with mesh sizes between 50,000 (grid 1) and 60 million cells (grid 5), are performed.

Each solution is advanced in time until it is statistically stationary. Statistics are obtained by averaging over the azimuthal direction and in time, and results for mean and root-mean-square quantities of normalized axial velocity, mixture fraction, and temperature are shown in Figure 2. The simulation results for the finer grids agree favorably with experiments. Once the simulation is statistically stationary, the Lyapunov exponent is calculated following the process outline in Section 2.1. One important aspect of the Lyapunov exponent is the speed at which it can be calculated. For the grid 4 inert case, two simulations, running for approximately 60 non-dimensional times, are required to calculate the Lyapunov exponent. In comparison, to obtain the results presented in Figure 2, statistics were collected over approximately 1500 non-dimensional units, corresponding to an increase in computational cost of 1250%.

3.2. *Effect of grid refinement*

To examine the dependence of the Lyapunov exponent on the mesh resolution, simulations on five different grids are performed for the non-reacting and reacting jets. In this study, the first four grids are generated by successively doubling the mesh resolution in all directions; grid 5 only refines the mesh resolution in axial and radial direction. Quantitative results for the Lyapunov exponent are shown in Table 3.2.

For the non-reacting jet, the relative increase in the Lyapunov exponent is much more pronounced for the coarser grids than for the finer grids. The Lyapunov exponent more than doubles from grid 1 to 3 and doubles again from grid 3 to grid 4. Convergence

Grid	$\lambda\tau_{\text{conv}}$ (inert)	$\lambda\tau_{\text{conv}}$ (reacting)
1	0.330	0.200
2	0.428	0.305
3	0.735	0.311
4	1.649	0.291
5	1.839	0.290

TABLE 1. Comparison of Lyapunov exponent for non-reacting and reacting jet-flow simulations. Grid numbers correspond to increasing grid refinement.

is nearly reached after testing the even finer grid 5. For the reacting jet, the variation in the Lyapunov exponent is much larger between grid 1 and grid 2, as compared to the difference between grid 2 and grid 3 (see Figure 3). This means that most of the dynamics is captured in grid 2. The statistical results, presented in Figure 2, also show this behavior. Results for grid 2 show statistics closer to the experimental values than for grid 1, and the statistical convergence is observed for grid 3 and above. These results show that grid 3 is suitable for capturing the global dynamics of the reacting jet, whereas at least grid 4 refinement is needed to simulate the global chaotic dynamics of the non-reacting jet, in agreement with the convergence of statistics in Figure 2. The physical reason for these two different resolution requirements is provided in the next section.

3.3. *Effect of combustion and heat-release on predictability*

In converting the normalized Lyapunov exponents for the finest grids into physical units, a predictability time of $t_{\text{p,reac}} \approx 650\ \mu$s $(3.45\tau_{\text{conv}})$ is obtained for the reacting jet, and $t_{\text{p,inert}} \approx 100\ \mu$s $(0.54\tau_{\text{conv}})$ is obtained for the inert jet. The physical reason for this difference is due to temperature increase by combustion and associated effects on density and viscous transport properties. A scaling of the effective Reynolds number can be calculated assuming a power law for the viscosity as $\text{Re} = \rho U_{\text{ref}} D_{\text{ref}}/\mu \sim \rho(T)/\mu(T) \sim (1/T)/T^{0.7} \sim T^{-1.7}$. Considering the present configuration that is operated with a nitrogen-diluted CH_4/H_2-mixture, with an effective temperature ratio of seven $\text{Re}_{\text{react}}/\text{Re}_{\text{inert}} = (T_a/T_{\text{ref}})^{-1.7} = 0.036$. Because the jet exit Reynolds number is 14,720, the effective Reynolds number of the flame reduces by a factor of 25. Combustion laminarizes the flow field, which in turn is responsible for a slower and more predictable flow. As noted previously, the Lyapunov time is representative of how long it takes for nearby Eulerian fields to diverge. The actual predictability time is a function of the Lyapunov time and would be dependent on how accurate the initial conditions provided are. For an error of around 1% for the present configuration, the predictability time is expected to be around this value. With higher accuracy, the predictability would become better. For example, the reacting cases simulated assume a perturbation of around 10^{-8} and have an overall predictability time of around 40 convective time scales before the separation reaches 1% of saturation (see Figure 3).

The increased predictability of the reacting flow, due to laminarization, suggests that it may be possible to determine the predictability time of reacting flows, using a lower Reynolds number inert jet, given the proper scaling relationships. Muniz & Mungal (2001) investigated inert jets at Reynolds numbers of 2,000 and 10,000 and reacting flows at

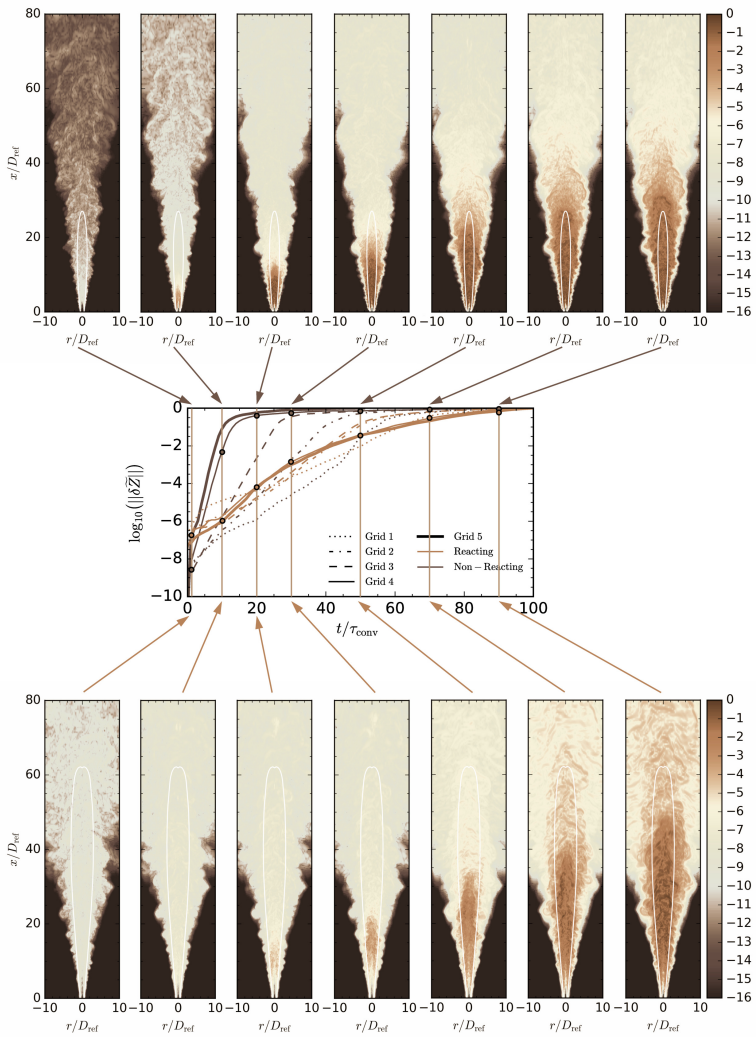

FIGURE 3. Separations for each grid and case. Lyapunov exponents are presented in Table 3.2. The contour plots correspond to the logarithm of the absolute value of the separation for mixture fraction, $\|\delta\widetilde{Z}\|$, between two simulations for grid 4 for (top) inert jet and (bottom) reacting jet. The white line indicates the Favre-averaged stoichiometric mixture fraction with $Z_{\mathrm{st}} = 0.167$.

Reynolds numbers of 10,000 and 37,500. In their work, several important observations were made: combustion reduced the local Reynolds number by a factor of 10 over the flame, turbulence intensities by up to 40% and increased the centerline velocities by a factor of 2 to 3. In the present study, similar behavior can be observed for the reacting jet as shown in Figure 2, suggesting the predictability of the reacting jet could be estimated based on a simple inert jet with a reduced Reynolds number. However, in practice this approach is not straightforward, as a large variation in the Reynolds number will be present due to the localized heating of the fluid. Thus, at the centerline near the nozzle, the effective Reynolds number will be equal to that of the pipe, whereas the effective Reynolds number in the shear layer, where the flame is stabilized, will be significantly

reduced. In the work of Tacina & Dahm (2000), an extension of the classical momentum diameter was developed for reacting flows, by replacing the exothermic reaction by an equivalent non-reacting flow. In this approach, the temperature of one fluid is increased based on the peak temperature and overall stoichiometry of the mixture. Good agreement of the effects of heat release were obtained in the near and far fields for momentum-dominated turbulent jet flames. A similar conclusion was obtained from the DNS study of Knaus & Pantano (2009), which determined that the effects of the heat release rate can be scaled out by using Favre-averaged large-scale turbulence quantities for flows of moderate Reynolds numbers. However, this approach is less suited for the dissipation subrange of the temperature spectra due to the strong nonlinearities present in combustion. Following the approach proposed by Tacina & Dahm (2000), the predictability of the reacting jet could be estimated based on an equivalent inert jet simulation with modified fluid temperatures.

3.4. *Application of the Lyapunov exponent to determining computational domain size*

In Section 3.2, the Lyapunov exponent has been shown to converge if the dynamics of the system are significantly resolved by the mesh. However, it is expected that the global dynamics of the system may also be a function of the computational domain size and shape. This expectation is tested by computing the Lyapunov exponent for a range of domains for the Grid 4 inert jet. Figure 4 presents the global separation for computational domains of various lengths, from x/D_{ref}=2.5 to 120. As can be seen in Figure 4, the jet dynamics varies significantly over the first $20D_{\mathrm{ref}}$ of the jet. Thus, if the computational domain is reduced to a length less than $20D_{\mathrm{ref}}$, it is expected that some of the important jet dynamics will be lost. In comparison, past x/D_{ref}=20, smaller changes in the jet are observed. Further, as these changes are due to the diffusion and lower velocity fluctuations are present, the positions downstream of this location will likely have a very small impact on the global separation, and thus on the global Lyapunov exponent. This behavior is confirmed in Figure 4, where the local separation converges for computational domains longer than $20D_{\mathrm{ref}}$, with a mean relative difference in the global separation of less than 11% for a domain of $20D_{\mathrm{ref}}$, when compared to the full domain. In addition, computational domains, with reduced radial length, were also compared with the trends agreeing with those of reducing the axial length.

In addition to comparing the normalized saturation curves to determine the impact of domain size on the Lyapunov exponent, an analysis of the global saturation level is also performed. With increasing domain size, saturation is observed at a lower threshold but occurs at approximately the same time scales. As the current approach calculates the Lyapunov exponent based on the global separation, the observed behavior is consistent with the previous observations reported in Section 3.2. If the computational domain is resolved to a significant level, and assuming that the computational domain includes the areas of high turbulences and areas which are sensitive to small perturbations, the growth of the separation is determined by the local flow conditions. Thus, increasing the computational domain does not influence the separation behavior. In comparison, the level at which saturation is observed is a strong function of the computational domain. The cause of this is that as the computational domain increases, the fraction of the domain that contains areas of low turbulence or areas which are not sensitive to perturbations increases. Thus, on a global scale, the average separation observed decreases resulting in saturation at a lower value. Note that this behavior is expected in geometries where turbulence, and thus sensitivity to small perturbations, is decaying. In processes in which strong turbulence is generated locally or develops, such as pipe flows, turbulence sepa-

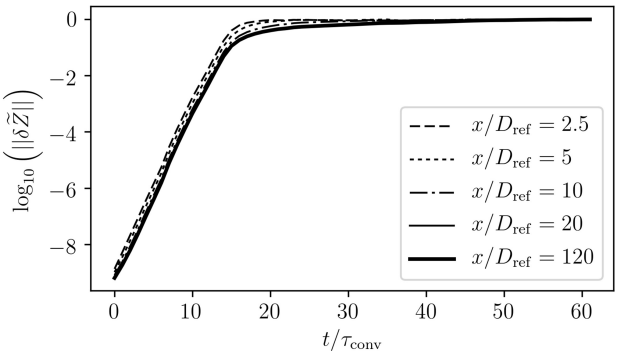

FIGURE 4. Simulation separation for different computational domains lengths from x/D_{ref}=2.5 to x/D_{ref}=120.

ration and boundary layer formation, this behavior is not expected, and the Lyapunov exponent may be a strong function of the size of the computational domain.

3.5. *Application of the Lyapunov exponent to assess flow-dependent properties*

In the previous sections, the global Lyapunov exponent was computed to determine the impact of various aspects (mesh resolution, computational domain and chemical source term) on the global dynamics of the system. However, the same principle can be applied to assess local flow-dependent properties. In the current section, the Lyapunov exponent analysis is applied to determine local areas of strong separation, corresponding to areas of high turbulence or high sensitivity to local conditions, which can be utilized to determine local grid refinement and areas which contain interesting dynamics.

The time evolution of the local separation, as a function of radial location at two axial heights, one close to the nozzle at x/D_{ref}=0.33 and one further downstream at x/D_{ref}=20, is presented in Figure 5. Several important characteristics can be observed from Figure 5. First, the behavior of the local separation, and conversely the Lyapunov exponent, is a strong function of radial location. In the laminar co-flow, the local separation remains close to machine precision over the simulation time, indicating that the co-flow is not sensitive to small changes in the initial or boundary conditions. In comparison, the dynamics in the jet core and shear layer are clearly visible in Figure 5, with the core of the jet less sensitive to small perturbations than the shear layer. Further, the behavior in the jet core and shear layer is relatively constant for t/τ_{conv} >20, demonstrating that saturation occurs very quickly and that the separation growth is strongly dependent on radial location near the nozzle. In comparison, further downstream at x/D_{ref}=20, a larger portion of the jet experiences similar rates of separation. However, at this location the level at which saturation occurs is approximately four orders of magnitude lower than at x/D_{ref}=0.33, indicating that the turbulence has decayed at this location.

A second dataset is calculated at two fixed radial locations, one at the centerline and one in the shear layer r/D_{ref}=0.5 for axial heights between x/D_{ref}=0 and x/D_{ref}=60, and is shown in Figure 6. Compared to the radial separation profiles, which reach saturation very quickly, an analysis of the separation growth shows that the time required to reach saturation is a strong function of axial height. As seen in Figure 6, the time to reach saturation increases with increased axial height. The rate of saturation growth as a function of axial height and non-dimensional time, represented by the dashed lines, is

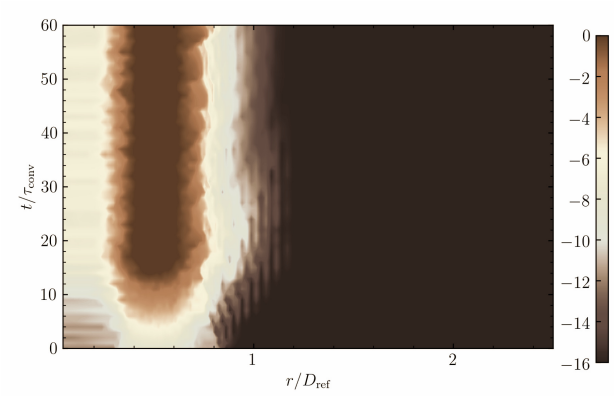

(a) x/D_{ref}=0.33

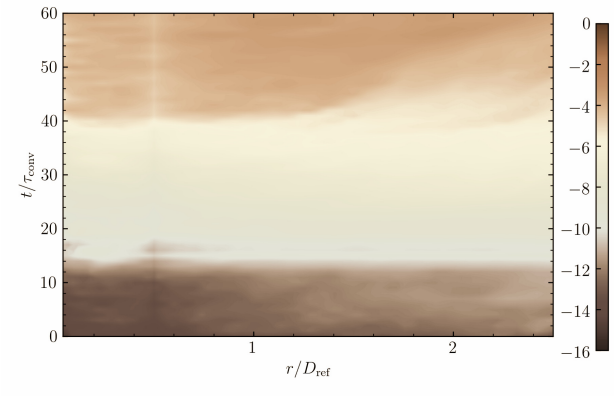

(b) x/D_{ref}=20

FIGURE 5. Simulation separation as a function of radial distance at two axial locations.

compared to the mean axial velocity. At both axial heights, the influence of the perturbation propagates downstream at approximately the local mean axial velocity. Thus, the Lyapunov exponent can be applied to estimate the time required for upstream turbulence to propagate downstream. This information is trivial for a simple stationary inert jet, but this process could be applied to transient simulations as a quick and easy method to determine how turbulent structures evolve for complex flows and geometries.

4. Conclusions

A dynamic metric based on the Lyapunov exponent is proposed to characterize the quality of LES and is applied to reacting and non-reacting turbulent jets. It is shown that the chaotic dynamics of LES of reacting and non-reacting flows behave like simple low-dimensional chaotic systems. The inverse of the Lyapunov exponent provides an estimate of the predictability time of a system, which is useful information in predicting rapid dynamic phenomena. For small perturbations, the predictability of the reacting and non-reacting flow scales with the Kolmogorov time scales.

The Lyapunov exponent asymptotically approaches a limit as the filter width and spatial resolution decrease in size (Nastac *et al.* 2017). When this happens, the numerical

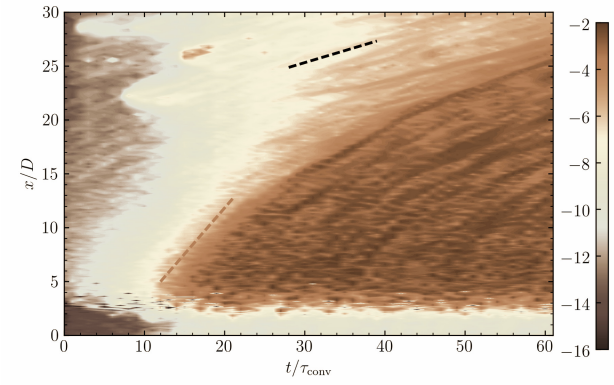

(a) r/D_{ref}=0

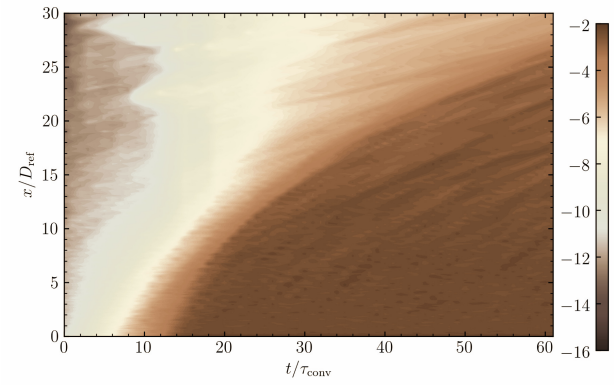

(b) r/D_{ref}=0.5

FIGURE 6. Simulation seperation as a function of axial heights at two radial locations.

grid and numerical model is suitable for capturing the chaotic turbulent dynamics. The Lyapunov metric is self-contained and model-free, which means it is consistent with the LES model adopted and does not require estimation of the subgrid scale variables. Combustion makes the jet dynamics more predictable in two ways. First, it enlarges the initial response time, which is the time that the exponential divergence of the chaotic dynamics takes to begin. Second, the exponential growth rate of the chaotic dynamics is lower due to the flame relaminarization, which decreases the effective Reynolds number.

An analysis of the local Lyapunov exponent demonstrates that this metric can also determine flow-dependent properties, such as areas of high turbulence and areas which are sensitive to small perturbations within the flow field. This information can be used to indicate areas where local grid refinement may be required. In addition, the impact of flow-dependent properties on the evolution of the flow can be assessed using the Lyapunov exponent and corresponding separation between two simulations. This information can provide an indication of the sensitivity of the simulation to initial conditions and boundary conditions, which may be important for the simulation of transient events. Finally, it is demonstrated that the global Lyapunov exponent can be utilized as a metric to determine if the computational domain is large enough to capture the dynamic nature of the flow. For the inert jet, the Lyapunov analysis correctly predicts that the area which

contains the majority of the dynamics is located close to the nozzle. It is observed that outside of this area, the flow does not have a significant impact on the dynamic nature of the system as measured by the Lyapunov exponent.

Acknowledgments

Financial support through the Ford-Stanford Alliance project #C2015-0590 is gratefully acknowledged. Computational resources supporting this work were provided by the National Energy Research Scientific Computing Center, a DOE Office of Science User Facility supported by the Office of Science of the U.S. Department of Energy under Contract No. DE-AC02-05CH11231.

REFERENCES

Aurell, E., Boffetta, G., Crisanti, A., Paladin, G. & Vulpiani, A. 1996 Growth of noninfinitesimal perturbations in turbulence. *Phys. Rev. Lett.* **77**, 1262–1265.

Bergmann, V., Meier, W., Wolff, D. & Stricker, W. 1998 Application of spontaneous Raman and Rayleigh scattering and 2D LIF for the characterization of a turbulent CH4/H2/N2 jet diffusion flame. *Appl. Phys. B* **66**, 489–502.

Boffetta, G., Cencini, M., Falcioni, M. & Vulpiani, A. 2002 Predictability: A way to characterize complexity. *Phys. Rep.* **356**, 367–474.

Bowman, C. T., Hanson, R. K., Davidson, D. F., Gardiner, W. C., Lissianski, V., Smith, G. P., Golden, D. M., Frenklach, M. & Goldenberg, M. 1997 GRI-Mech 2.11. Available from `http://www.me.berkeley.edu/gri-mech/`.

Celik, I. B., Cehreli, Z. N. & Yavuz, I. 2005 Index of resolution quality for large eddy simulations. *J. Fluid Eng.* **127**, 949–958.

Goldhirsch, I., Sulem, P.-L. & Orszag, S. A. 1987 Stability and Lyapunov stability of dynamical systems: A differential approach and a numerical method. *Physica D* **27**, 311–337.

Harlim, J., Oczkowski, M., Yorke, J. A., Kalnay, E. & Hunt, B. R. 2005 Convex error growth patterns in a global weather model. *Phys. Rev. Lett.* **94**, 228501.

Knaus, R. & Pantano, C. 2009 On the effect of heat release in turbulence spectra of non-premixed reacting shear layers. *J. Fluid Mech.* **626**, 67–109.

Meier, W., Barlow, R. S., Chen, Y. L. & Chen, J.-Y. 2000 Raman/Rayleigh/LIF measurements in a turbulent $CH_4/H_2/N_2$ jet diffusion flame: Experimental techniques and turbulence-chemistry interaction. *Combust. Flame* **123**, 326–343.

Mi, J., Nobes, D. S. & Nathan, G. J. 2001 Influence of jet exit conditions on the passive scalar field of an axisymmetric free jet. *J. Fluid Mech.* **432**, 91–125.

Muniz, L. & Mungal, M. G. 2001 Effects of heat release and buoyancy on flow structure and entrainment in turbulent nonpremixed flames. *Combust. Flame* **126**, 1402–1420.

Nastac, G., Labahn, J. W., Magri, L. & Ihme, M. 2017 Lyapunov exponent as a metric for assessing the dynamic content and predictability of large-eddy simulations. *Phys. Rev. Fluids* **2**, 094606.

Oseledets, V. I. 1968 Multiplicative ergodic theorem. Characteristic Lyapunov exponents of dynamical systems. *Tr. Mosk. Mat. Obs.* **19**, 179–210.

Pierce, C. D. & Moin, P. 2004 Progress-variable approach for large-eddy simulation of non-premixed turbulent combustion. *J. Fluid Mech.* **504**, 73–97.

Pope, S. B. 2004 Ten questions concerning the large-eddy simulation of turbulent flows. *New J. Phys.* **6**.

Schneider, C., Dreizler, A., Janicka, J. & Hassel, E. P. 2003 Flow field measurements of stable and locally extinguishing hydrocarbon-fueled jet flames. *Combust. Flame* **135**, 185–190.

Tacina, K. M. & Dahm, W. J. A. 2000 Effects of heat release on turbulent shear flows. Part 1. A general equivalence principle for non-buoyant flows and its application to turbulent jet flames. *J. Fluid Mech.* **415**, 23–44.

Temam, R. 1997 *Infinite-Dimensional Dynamical Systems in Mechanics and Physics*. Springer.

Vervisch, L., Domingo, P., Lodato, G. & Veynante, D. 2010 Scalar energy fluctuations in large-eddy simulation of turbulent flames: Statistical budgets and mesh quality criterion. *Combust. Flame* **157**, 778–789.